Journal of Power Sources 196 (2011) 9599–9604

Contents lists available at ScienceDirect

Journal of Power Sources

journal homepage: www.elsevier.com/locate/jpowsour

Improved hydrogen storage properties of Mg–V nanoparticles prepared by hydrogen plasma–metal reaction

Tong Liu [a,*], Tongwen Zhang [a], Chenggong Qin [a], Mu Zhu [a], Xingguo Li [b,**]

[a] Key Laboratory of Aerospace Materials and Performance (Ministry of Education), School of Materials Science and Engineering, Beihang University, Beijing 100191, China
[b] Beijing National Laboratory for Molecular Sciences (BNLMS), The State Key Laboratory of Rare Earth Materials Chemistry and Applications, College of Chemistry and molecular Engineering, Peking University, Beijing 100871, China

ARTICLE INFO

Article history:
Received 5 June 2011
Received in revised form 21 July 2011
Accepted 22 July 2011
Available online 29 July 2011

Keywords:
Hydrogen storage
Mg–V
Nanoparticles
Hydrogen plasma–metal reaction

ABSTRACT

The Mg–10.2 at.% V nanoparticles are prepared by hydrogen plasma–metal reaction (HPMR) method. These nanoparticles are made of Mg, VH_2 and a small amount of MgH_2. The Mg nanoparticles are hexagonal in shape with the particle size in the range of 50–150 nm. The VH_2 nanoparticles are spherical in shape with the particle size around 10 nm, and disperse on the surface of the Mg nanoparticles. After the hydrogen absorption, the mean particle size of MgH_2 decreases to 60 nm, while the V nanoparticles are still about 10 nm. The Mg–V composite nanoparticles can absorb 3.8 wt.% hydrogen in less than 30 min at 473 K and accomplish a high hydrogen storage capacity of 5.0 wt.% in less than 5 min at 623 K. They can release 4.0 wt.% hydrogen in less than 15 min at 573 K. The catalytic effect of the V nanoparticles and the nanostructure and the low oxide content of the Mg particles promote the hydrogen sorption process with the low hydrogen absorption activation energy of 71.2 kJ mol^{-1}.

1. Introduction

The constantly growing use of non-renewable fossil fuels gives rise to problems of both oil shortage and environmental degradation. Recently, as an ideal energy carrier candidate to replace the fossil fuel, hydrogen has drawn tremendous attentions from scientists and automotive industries. The key issue to realize the hydrogen economy is to develop a safe and efficient hydrogen storage approach. Solid-state hydrogen storage materials offer several advantages, including higher storage capacity and higher safety than the conventional approaches of liquefaction and compression [1]. Hydrogen storage materials through chemisorption include simple metal and intermetallic hydrides [2–4], and complex hydrides such as alanates, amides and boronates [5–7]. Among these hydrides, MgH_2 is still the most attractive one due to its high theoretical gravimetric capacity of 7.6 wt.%, abundance and low cost. Nevertheless, the practical application of MgH_2 has not been achieved as the result of its slow hydrogen sorption kinetics and high operational temperature [8].

In the past decades, many efforts have been made to improve the hydrogen sorption kinetics of MgH_2, such as reducing the particle size and crystallite size and adding the catalytic materials. Up to now, different kinds of transition metals and their oxides, including Fe, Ti, Ni, V, V_2O_5 and Cr_2O_3, to name a few, have been used as catalysts to enhance the sorption properties of Mg [9–15]. High energy ball milling (HEBM) is often adopted to disperse these catalysts effectively and produce nanostructured hydride particles. Holtz observed that the addition of 1 at.% Ni to Mg decreased the onset temperature of hydrogenation from 548 to 448 K and the hydrogen storage capacity increased by 50% [11]. Liang et al. [12] found that the ball milled MgH_2–5 at.% V nanocrystalline could desorb hydrogen completely within 1000 s at 523 K. Kondo and Sakurai demonstrated that Mg_2CaV_3 ternary alloy prepared by mechanical alloying for 10 h could absorb 3.3 wt.% even at 298 K [16]. On the other hand, the process of HEBM usually takes a long time, and it is also difficult to prevent the particles from oxidation and contamination. Moreover, the HEBM approach is unavailable to reduce the particle sizes of hydrides and catalysts to nano-scale.

The HPMR method is a novel vapor deposition process that is suitable for producing metallic nanoparticles industrially with high purity and low cost. So far, nanoparticles of various alloys and intermetallics have been fabricated by using HPMR approach, and the particle size can be tuned by controlling the hydrogen pressure and the current value [17–19]. Recently, the authors have synthesized the Mg–6.9 at.% Zn ultrafine particles that are made of Mg(Zn) solid solution and amorphous Mg–Zn alloy. These particles showed high hydrogen absorbing rate and high storage capacity due to the improved kinetics [20]. It is known that vanadium can absorb and release hydrogen under moderate pressure and temperature [21], and it is also an effective catalyst to improve the sorption properties of Mg [12]. Moreover, the production of nanoparticles

* Corresponding author. Tel.: +86 10 8231 6192; fax: +86 10 8231 4869.
** Corresponding author. Tel.: +86 10 6275 3691; fax: +86 10 6276 5930.
E-mail addresses: tongliu@buaa.edu.cn (T. Liu), xgli@pku.edu.cn (X. Li).

0378-7753/$ – see front matter © 2011 Elsevier B.V. All rights reserved.
doi:10.1016/j.jpowsour.2011.07.078

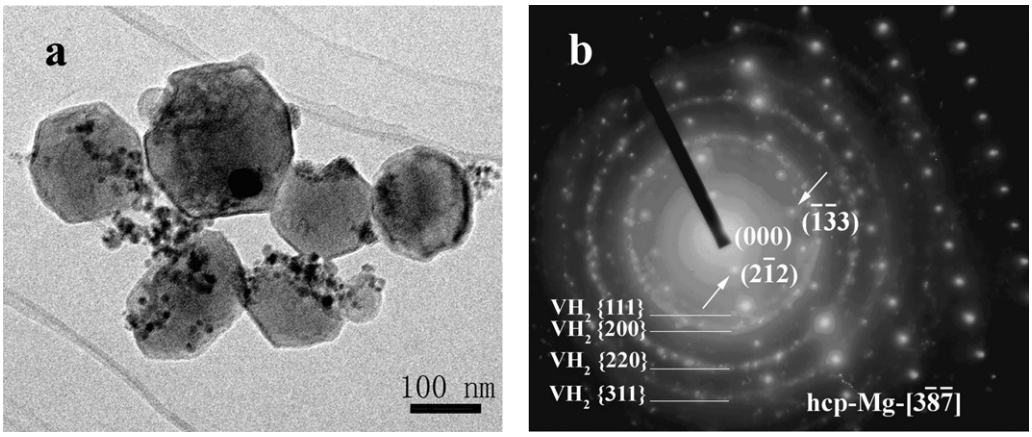

Fig. 1. TEM bright-field image of the as-prepared Mg–V nanoparticles (a) and the electron diffraction pattern of one big particle and several tens of small particles (b).

from Mg and V by HPMR will be quite different from the Mg–Zn system in that these two elements are immiscible [22]. Thus, the primary objective of the present study is to prepare the Mg–V composite nanoparticles using HPMR method and investigate the hydrogen sorption properties and the particle size and structure changes during the absorption and desorption cycle. To achieve good catalytic effect and high hydrogenation capacity, the target content of V is determined to be about 10 at.%.

2. Experimental

The equipment for producing nanoparticles primarily contains an arc melting chamber and a collecting system, which was described elsewhere [17]. The Mg–V nanoparticles were produced by arc melting Mg (purity >99.5%) ingot of 20 g and V (purity >99.5%) ingot of 20 g in a 50% Ar and 50% H_2 mixture of 0.1 MPa. The flow rate of the circulation gas for the collection of nanoparticles was 100 L min^{-1}. The arc current was selected as 80 A. Before the nanoparticles were taken out from the collection room, they were passivated with a mixture of argon and air to prevent the particles from burning.

The hydrogen desorption and absorption properties of the as-prepared Mg–V nanoparticles were evaluated using a Sievert-type apparatus. The volume of the reactor chamber was about 60 mL, and the error of the measurement was less than 5%. After the Mg–V nanoparticles of 100 mg were put into the Sievert reactor, the system was evacuated to 10^{-3} Pa. Then, the sorption kinetic curves at 473, 523, 573 and 623 K were measured after one absorption and desorption cycle at 673 K. A hydrogen pressure of 4 MPa was provided to make the Mg–V nanoparticles absorb hydrogen, and the desorption process was tested at each temperature under 10^{-1} Pa. A conventional pressure–volume–temperature technique was used to obtain the pressure–composition isotherm (*P–C–T*) curves of the Mg–V nanoparticles at 598, 623 and 648 K. Once the change of hydrogen pressure was less than 20 Pa s^{-1}, the hydrogen absorption and desorption measurements were considered as reaching the equilibrium.

The structural analysis of the Mg–V nanoparticles samples before and after the hydrogen sorption was carried out by X-ray diffraction (XRD) using a Rigaku X-ray diffractometer with monochromatic Cu K_α radiation. The morphology, size distribution and shape of the samples before and after the hydrogen sorption were observed by transmission electron microscopy (TEM) using JEOL-JSM-2100 at an accelerating voltage of 200 kV. The BET (Brunauer–Emmett–Teller) specific surface area was obtained from the nitrogen adsorption data using a Coulter Counter volumetric gas adsorption analyzer (Counter SA 3100) at 77 K. Before the BET measurement, the sample was activated by evacuating in vacuum at 393 K for 2 h.

3. Results and discussion

3.1. Particle feature

Fig. 1(a) displays the TEM image of the as-prepared Mg–V nanoparticles. It can be seen that there are two types of particles. The big particles vary from 50 to 150 nm with an average of about 100 nm. They have clear hexagonal shapes, which are the same as the pure Mg nanoparticles prepared with pure Mg by HPMR [23]. On the surface of each big particle, small particles of about 10 nm in spherical shape are dispersed. Fig. 1(b) shows the electron diffraction pattern of one big particle together with several tens of small particles. The point pattern can be indexed by the hexagonal structure of α-Mg (hcp) with the diffraction zone axis of [3 8̄ 7̄], indicating that the big particle is a single-crystal Mg. The ring pattern can be indexed by the fcc structure of VH_2, implying that the small particles belong to VH_2. This is quite different from the Mg–Zn system, where the Mg and Mg–Zn amorphous phases are included in one spherical particle [20]. The energy dispersive X-ray spectroscopy in Fig. 2 displays that the average V content in the Mg–V composite nanoparticles is 10.2 at.%. The lower V content in the as-prepared nanoparticles than that in the master ingots is due to the higher evaporation rate of Mg than that of V in the HPMR process.

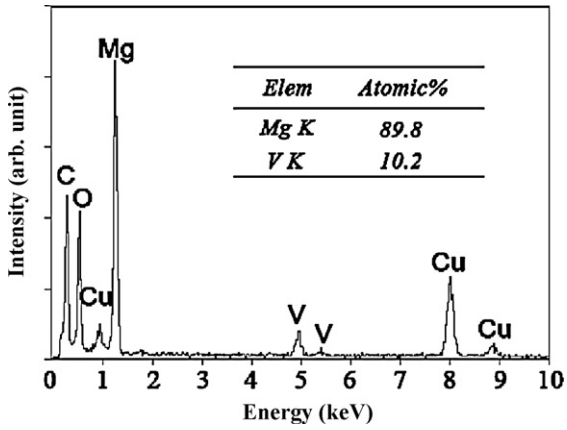

Fig. 2. The energy dispersive X-ray spectroscopy obtained from the Mg–V nanoparticles.

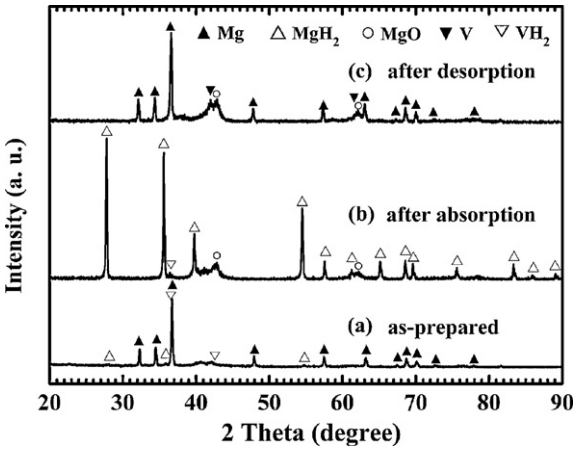

Fig. 3. X-ray diffraction patterns of the Mg–V nanoparticles (a) as-prepared, (b) after the absorption under 4 MPa hydrogen pressure at 673 K, and (c) after the hydrogen desorption under 10^{-1} Pa at 673 K.

Fig. 3 shows the XRD patterns of the as-prepared nanoparticles and the samples obtained after the hydrogen absorption and desorption at 673 K. It is found that the as-prepared sample contains dominantly α-Mg (hcp) together with a certain amount of fcc-VH_2, in excellent agreement with the TEM observation. It is surprising to find that 3 weak diffraction peaks of MgH_2 at 27.95°, 35.74° and 54.62°, are also discernable in Fig. 3(a). This means that a small amount of MgH_2 forms in the present work. Generally, no Mg hydride phase comes into being during the HPMR process when pure Mg or Mg–Zn alloy are used as the master materials [20,23], due to the poor formation kinetics of MgH_2. It is proposed that in the present work, the formation of MgH_2 is attributed to the catalytic effect of V nanoparticles dispersed on the surface of the Mg nanoparticles. The lattice constants of Mg calculated from the XRD data are $a = 3.209$ Å and $c = 5.211$ Å, the same as the standard data of pure α-Mg (JCPDS 35-0821), indicating that no V dissolves in Mg. This agrees with the Mg–V equilibrium binary diagram, where Mg and V are immiscible [22]. The metallic nanoparticles often become more pyrophoric than their corresponding coarse particles, and start to oxidize once exposed to air. It is worth to note that the diffraction peak of MgO around 42.9°, which usually appears in the Mg particles prepared by HPMR [23], cannot be detected in the present XRD pattern. This demonstrates that the addition of V effectively suppresses the pyrophoricity of Mg, and decreases the MgO content in the nanoparticles after the passivation process. From the XRD pattern in Fig. 3(b), it can be found that after the absorption process at 673 K, Mg and V elements in the Mg–V nanoparticles transform into MgH_2 and VH_2, respectively. It is observed from Fig. 3(c) that after the desorption at 673 K, MgH_2 dehydrogenates and changes completely into α-Mg, and VH_2 transforms into V. The peak of MgO at 42.9° is detectable in both Fig. 3(b) and (c), which is attributed to the fact that the nanoparticles were taken out of the chamber without sufficient passivation after the absorption and desorption processes.

Fig. 4 shows the TEM image of the Mg–V nanoparticles after the absorption. It is interesting to find that after the hydrogen absorption, the MgH_2 nanoparticles are no longer in the hexagonal shape but are broken into smaller quasi-spherical particles with an average size of about 60 nm. It is also shown in Fig. 4 that after the absorption, the fine black particles, known as VH_2, is still around 10 nm, almost the same as the as-prepared sample. They are homogeneously distributed on the surface of the MgH_2 nanoparticles. The nitrogen adsorption–desorption isotherm curves of the as-prepared and the hydrogenated Mg–V samples are displayed in Fig. 5. It is clear that as the consequence of the reduction in the

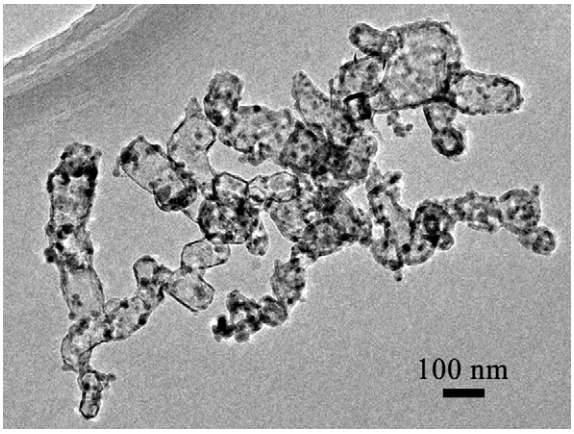

Fig. 4. Bright field electron image of Mg–V nanoparticles after the hydrogen absorption under 4 MPa hydrogen pressure at 673 K.

particle size of MgH_2, the surface area of the hydrogenated sample measured by BET is 20.5 $m^2\,g^{-1}$, nearly twice as much as that of the as-prepared sample, 10.3 $m^2\,g^{-1}$.

On the basis of the analysis above, the formation of the Mg–V composite nanoparticles by HPMR and the hydrogen absorption and desorption processes can be summarized into the following equations, respectively:

$$Mg + V + H_2 \rightarrow Mg + MgH_2 + VH_2 \quad (1)$$

$$Mg + V + H_2 \rightarrow MgH_2 + VH_2 \quad (2)$$

$$MgH_2 + VH_2 \rightarrow Mg + V + H_2 \quad (3)$$

3.2. Hydrogen storage properties

The activation treatment through annealing at 673 K in vacuum and in hydrogen for several cycles is often required for the micro-size Mg particles. However, even after the activation, Mg at microscale can absorb only 1.5 wt.% hydrogen within 2 h at a temperature as high as 673 K [8]. Fig. 6(a) shows the hydrogen absorption curves of the Mg–V composite nanoparticles at different temperatures. It can be observed that after one absorption and desorption cycle at 673 K under 4 MPa hydrogen and vacuum (10^{-1} Pa), the Mg–V nanoparticles can absorb hydrogen even at 473 K and reach a value of 3.8 wt.% in less than 30 min, quite superior to the Mg–Zn nanoparticles that absorb only 2.3 wt.% in 55 min at the same temperature [20]. This result is comparable with the very recent report that Mg nanopar-

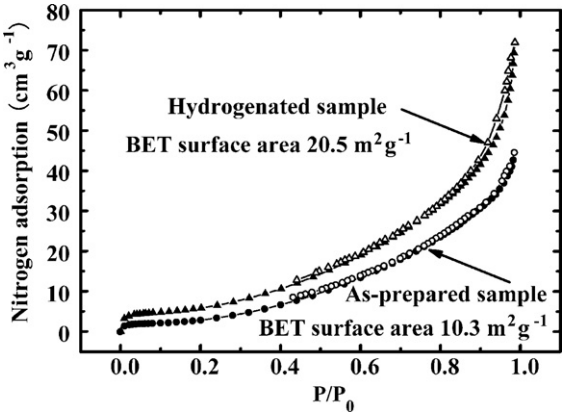

Fig. 5. Nitrogen adsorption–desorption isotherm curves of the as-prepared and the dehydrogenated Mg–V samples.

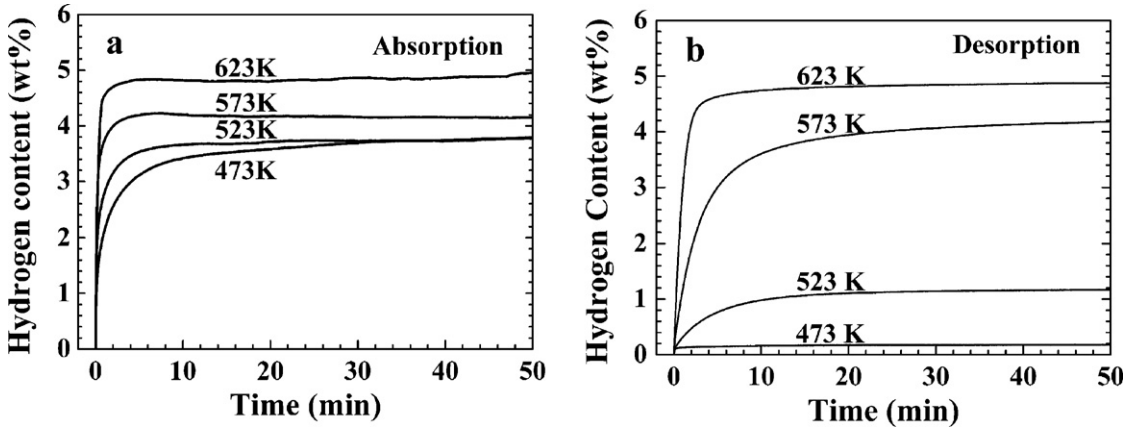

Fig. 6. Hydrogen absorption curves (a) and desorption curves (b) of the Mg–V nanoparticles at 473, 523, 573 and 623 K under 4 MPa hydrogen pressure after one absorption and desorption cycle at 673 K.

ticles with a mean particle size of 38 nm can absorb nearly 4 wt.% in 40 min at 493 K [24]. However, the Mg–V nanoparticles show higher hydrogenation rate due to the catalytic effect of the V nanoparticles, especially at the initial stage. It is also found from Fig. 6(a) that the hydrogen absorption rate increases with increasing temperature from 473 to 623 K. At 523, 573 and 623 K, the hydrogen absorption content enlarges remarkably with time at the initial absorption stage and reaches a saturation value of 3.8, 4.2 and 5.0 wt.% in 5 min, respectively. Fig. 6(b) shows the hydrogen desorption curves of the Mg–V nanoparticles at different temperatures. It is found that the hydrogen desorption content rises remarkably with time at the initial desorption stage and reaches a saturation value of 4.9 wt.% H in 10 min at 623 K. Even at 573 K, the Mg–V nanoparticles can dehydrogenate 4.0 wt.% H in 15 min, nearly the same as the absorbed value at 573 K.

It is well known that the hydrogenation rate of Mg is affected by several factors. Firstly, the surface of pure magnesium without catalytic additives requires a very high energy for the dissociation of H_2. In the present work, the V nanoparticles dispersed on the surface of Mg particles act as a catalyst to decrease the activation energy to dissociate H_2 and improve the hydrogen sorption kinetics of Mg nanoparticles. Secondly, the formation rate of MgH_2 on the Mg surface and the diffusion rate of hydrogen atoms within MgH_2 are the critical factors to impact the hydrogenation capacity and kinetics, due to the fact that the diffusion coefficient of H in MgH_2 is much smaller than that in Mg [25]. It was also reported that the hydrogenation rate of the magnesium decreased with increasing hydride layer thickness [26]. In this work, the nano-scale particle size decreases the thickness of MgH_2, accelerates the H diffusion and improves the hydrogen sorption kinetics of Mg. Additionally, it is known that the oxide layer of Mg particles prevents hydrogen from transporting into Mg. In this work, the decrease of oxide content in the Mg–V composite nanoparticles enhances the sorption of H on the surface of the Mg nanoparticles. Thus, the high hydrogen sorption rate is attributed to the combined effects of the catalytic V nanoparticles, and the nanostructure and the decreased oxide content of Mg particles.

The activation energy for hydrogen absorption is usually calculated from the JMAK (Johnson–Mehl–Avrami–Kolmogorov) model and the Arrhenius theory. On the basis of JMAK model, the hydrogen absorption kinetics can be expressed in the following linear equation:

$$\ln[-\ln(1-\alpha)] = \eta \ \ln k + \eta \ln t \tag{4}$$

where α is the fraction transformed at time t, k is an effective kinetic parameter, η is the Avrami exponent of reaction order. For the experimental data of 473, 523, 573 and 623 K, by plotting $\ln[-\ln(1-\alpha)]$ vs. $\ln(t)$, each temperature provides a straight line with a slope η and an intercept $\eta \ln(k)$. After calculating the rate constant k from the η value, the apparent activation energy for the absorption process is evaluated from the Arrhenius equation:

$$k = A \ \exp\left(\frac{-E_a}{RT}\right) \tag{5}$$

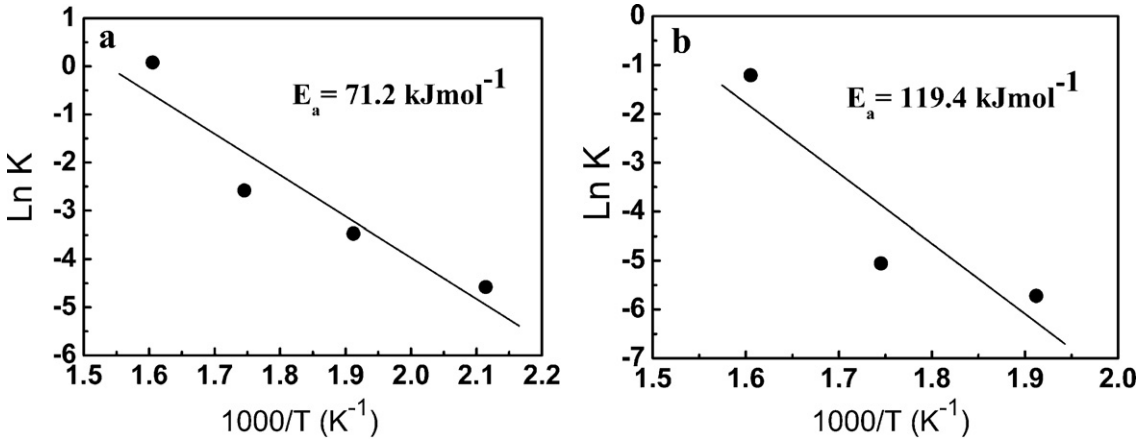

Fig. 7. Absorption plot (a) and desorption plot (b) of $\ln k$ vs. $1000/T$ of the Mg–V nanoparticles.

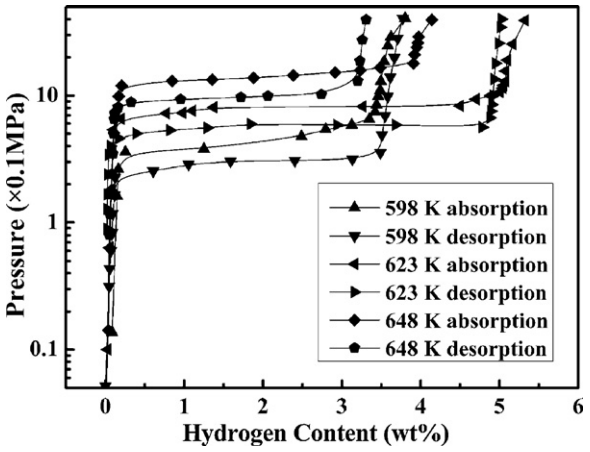

Fig. 8. Pressure–composition isotherm curves of the Mg–V nanoparticles at 598, 623 and 648 K.

where A is a temperature-independent coefficient, E_a is the apparent activation energy, R is the gas constant (8.314472 J mol^{-1} K^{-1}), and T is the absolute temperature. The absorption plot of ln(k) vs. 1000/T is shown in Fig. 7(a), and the calculated hydrogen absorption activation energy of the Mg–V nanoparticles is 71.2 kJ mol^{-1}, which is quite smaller than that of the 25 nm Mg particles, 122 kJ mol^{-1} [24]. By using the same approach, the desorption plot of ln(k) vs. 1000/T for the experimental data of 523, 573 and 623 K is shown in Fig. 7(b), and the hydrogen desorption activation energy of the Mg–V nanoparticles is 119.4 kJ mol^{-1}. This value is slightly larger than that of the Mg particles catalyzed with Ni nanoparticles, 94 kJ mol^{-1}, but is quite lower than that of non-catalyzed Mg particles, 323 kJ mol^{-1} [27].

Fig. 8 shows the P–C–T curves of the hydrogen absorption–desorption for the Mg–V nanoparticles at 598, 623 and 648 K. The hydrogen pressures of the absorption plateaus are 1.41 MPa at 648 K, 0.81 MPa at 623 K and 0.44 MPa at 598 K. The hydrogen pressures of the desorption plateaus are 0.96 MPa at 648 K, 0.59 MPa at 623 K and 0.30 MPa at 598 K. From these data, the Van't Hoff Plots (ln P vs. 1/T) for both absorption and desorption of the Mg–V nanoparticles are built in Fig. 9. According to the fitting line from the experimental data, the Van't Hoff equation for the absorption is $\ln(P) = -8.93/T + 18.74$. The obtained value of the formation enthalpy (ΔH_{abs}) for the Mg–V nanoparticles is −74.3 kJ mol^{-1}, comparable with the formation enthalpy for the Mg micro-particles reported by other works [28,29]. The Van't Hoff equation for the desorption is $\ln(P) = -8.94/T + 18.39$. The decomposition enthalpy (ΔH_{des}) for the Mg–V nanoparticles is evaluated

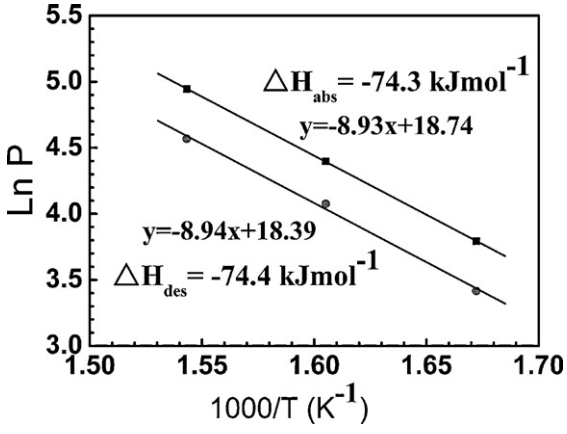

Fig. 9. Van't Hoff plots for the Mg–V nanoparticles.

to be −74.4 kJ mol^{-1}, similar with that of the Mg micro-particles [30]. This implies that the addition of V to Mg does not alter the thermodynamics of the hydrogenation process, but improve the sorption kinetics. The Mg–V composite nanoparticles with high sorption kinetics and storage capacity, and relatively low hydrogenation temperature, are a promising candidate for hydrogen storage.

4. Conclusions

The Mg–10.2 at.% V composite nanoparticles were prepared from the Mg and V ingots by HPMR method. The Mg nanoparticles are hexagonal in shape with an average particle size of 100 nm. The spherical VH_2 nanoparticles with a mean diameter of 10 nm disperse evenly on the surface of the Mg nanoparticles. After the hydrogen absorption, the MgH_2 nanoparticles decrease to 60 nm, while the V nanoparticles are still about 10 nm.

The Mg–V composite nanoparticles can absorb 3.8 wt.% hydrogen in less than 30 min even at 473 K, and accomplish a high hydrogen storage capacity of 5.0 wt.% in less than 5 min at 623 K. They release 4.0 wt.% hydrogen in less than 15 min at 573 K. The catalytic effect of the V nanoparticles, and the nanostructure and the low oxide content of the Mg particles result in the low hydrogen absorption and desorption activation energies of 71.2 and 119.4 kJ mol^{-1}, respectively. The enhanced hydrogen sorption rate and storage capacity are due to the improved kinetics rather than the change in enthalpy.

Acknowledgements

The authors acknowledge the support of this work by MOST of China (No. 2011AA03A408 and 2010CB631301), the Specialized Research Fund for the Doctoral Program of Higher Education (No. 20091102120009), and the Aeronautical Science Foundation of China (No. 2009ZF51062).

References

[1] B. Sakintuna, F. Lamari-Darkrim, M. Hirscher, Int. J. Hydrogen Energy 32 (2007) 1121–1140.
[2] K.J. Jeona, A. Theodoreb, C.Y. Wu, J. Power Sources 183 (2008) 693–700.
[3] A. Demircan, M. Demiralp, Y. Kaplan, M.D. Mat, T.N. Veziroglu, Int. J. Hydrogen Energy 30 (2005) 1437–1446.
[4] M.V. Simičić, M. Zdujić, R. Dimitrijević, L. Nikolić-Bujanović, N.H. Popović, J. Power Sources 158 (2006) 730–734.
[5] S.I. Orimo, Y. Nakamori, J.R. Eliseo, A. Züttel, C.M. Jensen, Chem. Rev. 107 (2007) 4111–4132.
[6] P. Chen, Z. Xiong, J. Luo, J. Lin, K.L. Tan, Nature 420 (2002) 302–304.
[7] J. Yang, A. Sudik, C. Wolverton, J. Phys. Chem. C 111 (2007) 19134–19140.
[8] A. Zaluska, L. Zaluski, J.O. Strom-Olsen, J. Alloys Compd. 288 (1999) 217–225.
[9] J.A. Puszkiel, P.A. Larochette, F.C. Gennari, J. Power Sources 186 (2009) 185–193.
[10] S. Rousselot, D. Guay, L. Roué, J. Power Sources 195 (2010) 4370–4374.
[11] R.L. Holtz, M.A. Imam, J. Mater. Sci. 34 (1999) 2655–2663.
[12] G. Liang, J. Huot, S. Boily, A. Van Neste, R. Schulz, J. Alloys Compd. 292 (1999) 247–252.
[13] Y. He, Y. Zhao, Nanotechnology 20 (2009) 204008.
[14] K.S. Jung, E.Y. Lee, K.S. Lee, J. Alloys Compd. 421 (2005) 179–184.
[15] M.Y. Song, J.L. Bobet, B. Darriet, J. Alloys Compd. 340 (2002) 256–262.
[16] T. Kondo, Y. Sakurai, J. Alloys Compd. 417 (2006) 164–168.
[17] X.G. Li, A. Chiba, S. Takahashi, J. Magn. Magn. Mater. 170 (1997) 339–345.
[18] T. Liu, H.Y. Shao, X.G. Li, Intermetallics 12 (2004) 97–102.
[19] T. Liu, H.Y. Shao, X.G. Li, Nanotechnology 14 (2003) 542–545.
[20] T. Liu, T.W. Zhang, X.Z. Zhang, X.G. Li, Int. J. Hydrogen Energy 36 (2011) 3515–3520.
[21] D.L. Cummings, G.J. Powers, Ind. Eng. Chem. Process Des. Dev. 13 (1974) 182–192.
[22] B.M. Thaddeus, L.M. Joanne, H.B. Lawrence, B. Hugh, K. Linda, Binary Alloy Phase Diagrams, American Society for Metals, 1986.
[23] T. Liu, Y.H. Zhang, X.G. Li, Scripta Mater. 48 (2003) 397–402.

[24] N.S. Norberg, T.S. Arthur, S.J. Fredrick, A.L. Prieto, J. Am. Chem. Soc. 28 (2011) 10679–10681.
[25] D.S. Sholl, J. Alloys Compd. 446 (2007) 462–468.
[26] X. Yao, Z.H. Zhu, H.M. Cheng, G.Q. Lu, J. Mater. Res. 23 (2008) 336–340.
[27] N. Hanada, T. Ichikawa, H. Fujii, J. Phys. Chem. B 109 (2005) 7188–7194.
[28] J.F. Stampfer, C.E. Holley, J.F. Suttle, J. Am. Chem. Soc. 82 (1960) 3504–3508.
[29] W. Klose, V. Stuke, Int. J. Hydrogen Energy 20 (1995) 309–316.
[30] R.A. Varin, T. Czujko, Z.S. Wronski, Nanomaterials for Solid State Hydrogen Storage, Springer Science Business Media, 2009.